Impact of Hydrogen Concentration on the Local Structure of Yttrium In Photochromic Yttrium Oxyhydride

H. Arslan[1], A. Kuzmin[1], I. Pudza[1], and S. Karazhanov[1,2*]

[1] Institute of Solid State Physics, University of Latvia, LV-1063 Riga, Latvia
[2] Institute for Energy Technology, P.O. Box 40, NO-2027 Kjeller, Norway

Abstract

We report a systematic study of the relationship between structure and photochromic activity in yttrium oxyhydride (YHO) thin films deposited by DC magnetron sputtering under different ratios of ionization gas (Ar) and reactant gas (H_2) flows. The best photochromic performance was observed for intermediate ratios $Ar/H_2 \approx 9$-12. Decreasing the Ar/H_2 ratio to about 5 promotes film growth with a (200) texture and suppresses photochromic activity. On the contrary, increasing the Ar/H_2 ratio to about 19 results in a dark-colored film without photochromic activity, exhibiting a metallic-like environment similar to Y foil or yttrium hydride. The local atomic structure and oxidation state of yttrium cations were probed using Y K-edge X-ray absorption spectroscopy. No shift in the absorption edge position was found under different deposition and illumination conditions, indicating an average $Y^{2.5+}$ oxidation state in YHO films. Analysis of extended X-ray absorption fine structure confirms that, while yttrium ions are on average arranged on a face-centred cubic lattice, local structural distortions induce a splitting of the second coordination shell of yttrium, well visible in both transparent and dark film states. These findings suggest that photochromism in YHO is not driven by changes in the average electronic structure of yttrium ions. The previously reported reduction of the yttrium charge may instead result from light-induced anion vacancy formation and defect migration.

Keywords: Photochromic yttrium oxyhydride, magnetron sputtering, X-ray absorption spectroscopy, X-ray diffraction.

* Corresponding author. E-mail: smagul.karazhanov@ife.no

Highlights:

- No shift in the Y K-edge absorption edge position was found under different deposition and illumination conditions, indicating an average $Y^{2.5+}$ oxidation state in yttrium oxyhydride thin films.
- Analysis of the Y K-edge extended X-ray absorption fine structure spectra confirms that, while yttrium ions are on average arranged on a face-centred cubic lattice, local structural distortions induce a splitting of the second coordination shell of yttrium.
- X-ray diffraction measurements reveal that decreasing the Ar/H_2 ratio during DC magnetron sputtering promotes film growth with a (200) texture and suppresses photochromic activity.
- The lack of detectable changes in average yttrium ion oxidation state and the splitting of the second coordination shell of yttrium, observed by X-ray absorption spectroscopy, implies that photochromism in yttrium oxyhydride thin films may result from light-induced anion vacancy formation and defect outdiffusion mechanisms.

1. Introduction

Yttrium oxyhydride (YHO) with the chemical formula $YH_{3-2x}O_x$ exhibits photochromic properties under ambient conditions [1]. In its transparent state, YHO shows a transmittance greater than 85%, while in the photodarkened state, transmittance drops to approximately 20%. The coloration process occurs within ~10 minutes, and bleaching takes less than 20 minutes [2]. Unlike other inorganic oxides such as WO_3 [3] and MoO_3 [4], which require thermal treatment in an oxidizing atmosphere to reverse photodarkening [5], YHO undergoes both photodarkening and bleaching at room temperature without the need for external energy input. This reversible photochromic behavior makes YHO a promising candidate for applications in smart window facades, goggles, helmet visors, and automotive roof glass [6, 7].

In molecular and solid-state systems, the photochromism is often attributed to light-induced local structural rearrangements. These may include bond breaking/forming [8], local lattice distortions, changes in coordination geometry, defect formation or migration, and structural rearrangement [9, 10]. Such changes can be reversible and contribute to the observed photochromic response. Extended X-ray Absorption Fine Structure (EXAFS) spectroscopy is a powerful technique for probing the local structural environment around specific atomic species, particularly in disordered or amorphous materials. EXAFS provides key structural parameters such as interatomic distances, coordination numbers, disorder factors, and the identity of neighboring atoms.

Despite extensive research, the origin of photochromism in YHO remains an open question. Several models have been proposed, including those suggesting that photochromism arises from light-induced local structural rearrangements [9, 10], while an X-ray diffraction (XRD) study demonstrated that the process is accompanied by a lattice expansion/contraction [11]. The earlier theoretical study [11] also suggested a possible reduction of Y^{3+} to Y^{2+} upon illumination [11], a hypothesis later supported by nuclear magnetic resonance (NMR) spectroscopy [12]. Interestingly, X-ray absorption near-edge structure (XANES) and EXAFS studies [9,10] suggest that photochromism in YHO is not associated with a significant change in the average oxidation state of yttrium cations. In contrast, NMR studies of analogous systems have shown partial conversion of Sc^{3+} to Sc^{2+}, with a broad distribution of valence states and approximately 10% of Sc cations undergoing reduction—a substantial fraction [12].

Deposition conditions play a critical role in determining the composition and photochromic behavior of YHO films. Variations in chamber pressure and Ar/H_2 gas flow ratios lead to differences in hydrogen and oxygen concentrations, which are known to be anticorrelated [13]. If photochromism in YHO is indeed linked to changes in the oxidation state of yttrium, then compositional variations could influence this behavior even in the absence of light. The photochromic response depends strongly on film composition, which can be tuned via deposition pressure, gas flow ratios, oxidation atmosphere, and temperature [13-15]. For instance, increasing the deposition pressure enhances the [O]/[Y] ratio while simultaneously reducing the [H]/[Y] ratio [13]. The interplay between hydride and oxide anions also affects anion vacancy concentrations, and photochromism is observed within the range $0.45<[O]/[Y]<1.5$ [15, 16]. Using ion beam analysis and optical characterization, a correlation between film composition and photochromic performance has been established [15-17].

Previous X-ray absorption spectroscopy (XAS) studies have typically focused [9, 10] on samples produced under a single set of deposition conditions. Given that both photochromic and structural properties of YHO are composition-dependent and that oxygen and hydrogen concentrations are anticorrelated, XAS measurements on films deposited under varied conditions (e.g., different chamber pressures and Ar/H_2 ratios) are expected to yield deeper insights into the oxidation state of yttrium and its local structural environment. Such

investigations could reveal new relationships between deposition parameters, yttrium oxidation states, and structural rearrangements.

This study aims to investigate the local structural arrangement and oxidation state of yttrium cations in YHO films deposited under varying chamber pressures and Ar/H_2 gas flow ratios, using the Y K-edge XAS spectroscopy.

2. Methods

Yttrium oxyhydride ($YH_{3-2x}O_x$) thin films were deposited on soda-lime glass substrates using a two-step process [18] via DC magnetron sputtering (Leybold Optics A550V7). In the first step, yttrium was sputtered in a reactive H_2/Ar atmosphere, forming substoichiometric yttrium hydride (YH_{2-x}). The deposition of YH_x films was carried out at room temperature in a mixed argon–hydrogen atmosphere (Table 1) using a 6 mm thick metallic yttrium target (purity 99.9%, size 125 mm × 600 mm) supplied by Plasmaterials. During the deposition process, the substrate temperature increased to ~3 °C.

In the second step, the as-deposited YH_{2-x} films were exposed to ambient air at ~22 °C, ~1 atm pressure, and ~35% relative humidity, resulting in oxidation and the formation of $YH_{3-2x}O_x$. By varying the H_2/Ar gas flow ratio and chamber pressure during deposition, YH_{2-x} films with different hydrogen concentrations were obtained. These variations influence the films' adsorption energies toward environmental gases such as O_2, CO_2, and H_2O. Consequently, oxidation in ambient air produces $YH_{3-2x}O_x$ films with distinct oxygen and hydrogen contents, depending on the initial hydrogen concentration of the precursor YH_{2-x} films.

The resulting $YH_{3-2x}O_x$ samples used in this study are labeled S3 through S8, and the deposition parameters for each sample are summarized in Table 1. Among these, samples S3, S4, and S6–S8 are transparent in the visible range and exhibit photochromic behavior, whereas sample S5 appears black and corresponds to a slightly oxidized YH_{2-x} composition. Coloration of the YHO thin films in certain places was achieved using a UVA LED source with a wavelength of 400 nm. The samples were placed on a rotating table and illuminated from one side during continuous rotation for the same duration. The result was the formation of dark stripes.

For comparison, metallic yttrium (Y) and fully oxidized yttrium oxide (Y_2O_3) thin films were also deposited via magnetron sputtering at room temperature under a range of ultra-low to moderate oxygen partial pressures. These reference samples were used to investigate the transition kinetics from metallic Y to Y_2O_3. Specific oxygen partial pressures and deposition parameters for these reference films are detailed in Ref. [19].

Table 1. Preparation conditions of yttrium oxyhydride thin films and the average crystallite size D.

Sample	Power (W)	Voltage (V)	Current (A)	Base Pressure (Pa)	Deposition Pressure (Pa)	Ar/H_2 (Const./Var.)	D (nm)
S3	1000 (±2)	168 (±1)	6.0 (±0.1)	~ 2.0E-06	1.1	9.4	5.2 (±0.2)
S4	1000 (±2)	182 (±2)	5.5 (±0.1)	~ 2.0E-06	1.1	4.7	9.4 (±0.2)
S5	1000 (±2)	164 (±1)	6.0 (±0.1)	~ 2.0E-06	1.1	18.8	-
S6	1000 (±2)	166 (±1)	6.0 (±0.1)	~ 2.0E-06	1.0	9.4	5.2 (±0.2)
S7	1000 (±2)	168 (±2)	6.0 (±0.1)	~ 2.0E-06	1.0	8	6.4 (±0.2)

S8	1000 (±2)	166 (±1)	6.0 (±0.1)	~ 2.0E-06	1.0	11.4	5.0 (±0.2)

To facilitate a wide-range XRD investigation (2θ, 20-120°) for use in Rietveld refinement, a portion of the deposited thin film was scraped off the surface, resulting in powdered specimens. The powder and thin film specimens were stored in a nitrogen atmosphere glovebox, in which O_2 and H_2O concentrations were less than 0.1 ppm, to ensure their integrity and enable subsequent analysis.

XRD patterns of the YHO thin films (S3-S8) were collected using a Rigaku MiniFlex 600 benchtop X-ray powder diffractometer, having a Bragg-Brentano θ–2θ geometry and equipped with the copper anode X-ray tube (Cu Kα radiation at 40 kV and 15 mA). A D/teX Ultra 1D high-speed silicon strip detector was used to acquire data with a step size of Δ(2θ) = 0.005°, covering a 2θ range from 10° to 90°. The average crystallite size D of the YHO thin films was estimated from the broadening of selected Bragg reflections using the Scherrer method, which relates diffraction peak width to coherent domain size. For a given diffraction peak, the crystallite size was calculated using the Scherrer equation:

$$D = \frac{K \times \lambda}{\beta \times \cos\theta},$$

where K is the shape factor (taken as 0.9 for approximately spherical nanocrystallites), λ is the X-ray wavelength of the Cu Kα radiation ($\lambda = 1.5406$ Å), β is the full width at half maximum (FWHM) of the diffraction peak after subtracting instrumental broadening, and θ is the Bragg angle. This analysis was performed using the most intense non-overlapping reflections of the cubic YHO phase. The Scherrer equation provides an estimate of the coherent scattering domain size and is widely applied in nanocrystalline thin-film systems where peak broadening arises primarily from finite crystallite size rather than microstrain. Although it does not account for lattice strain or defect-induced broadening, the method is sufficient for comparing the relative crystallite sizes across the film series. The calculated values, summarized in Table 1, show that films deposited at intermediate Ar/H_2 ratios exhibit smaller crystallites (5-6.5 nm), whereas films grown at higher hydrogen partial pressure (e.g., sample S4) show larger crystallites (~9 nm), consistent with the observed trends in peak sharpening and texture evolution.

X-ray absorption measurements were performed at the DESY PETRA-III P65 Applied XAFS undulator beamline [20]. The storage ring operated at an energy of 6.08 GeV and a current of 120 mA in top-up 480-bunch mode. The beamline optics included two Rh-coated silicon plane mirrors, used to suppress higher harmonics, and a fixed-exit Si(111) double-crystal monochromator. The Y K-edge X-ray absorption spectra were recorded in continuous-scan fluorescence mode for both transparent and UVA colored (dark) parts of the samples. The intensities of the incident and fluorescent X-rays were monitored with an ionisation chamber and the passivated implanted planar silicon (PIPS) detector, respectively. The PIPS detector was placed at the 90° angle relative to the incoming X-ray beam. The Y_2O_3 powder (prepared as a pellet with cellulose) and a yttrium foil were used as references. The XANES and EXAFS regions of the spectra were extracted using the XAESA code [21], following standard procedures [22].

The information on the local environment in the YHO thin films was obtained from the analysis of the Y K-edge EXAFS spectra using reverse Monte Carlo (RMC) simulations with the evolutionary algorithm approach, as implemented in the EvAX code [23, 24]. We used the same approach as in our previous studies of the YHO materials [9, 19, 25] and bulk Y_2O_3 [26]. Briefly, the RMC simulations were performed for a cubic box of a size of $4a \times 4a \times 4a$ unit cells of YHO (a = 5.402 Å). During the RMC simulations, the atoms in the box were randomly displaced till a good agreement between theoretical and experimental EXAFS spectra in the

wavelet space [27] was achieved. The EXAFS spectra for each yttrium atom in the simulation box were obtained within ab initio real-space multiple-scattering formalism using the FEFF8.5L code [28]. The RMC simulations were repeated ten times for each sample using different pseudorandom sequences of numbers to obtain reasonable statistics. The partial radial distribution functions (RDFs) g(*r*) for Y–O and Y–Y atom pairs were calculated from the coordinates of atoms in the simulation box.

3. Results and discussion

Two sets of YHO thin films were investigated, deposited at chamber pressures of 1.1 Pa and 1.0 Pa, respectively, using different Ar/H_2 gas flow ratios (Table 1). These variations in deposition conditions yield YH_{2-x} precursor films with distinct hydrogen concentrations. Upon exposure to ambient air after deposition, the films undergo oxidation to form YHO. The Ar/H_2 gas flow ratio and chamber pressure influence not only the hydrogen content and porosity of the as-deposited films, but also affect subsequent gas adsorption energetics and oxidation kinetics [13]. As a result, the final oxygen concentration in the YHO films depends on the initial deposition parameters.

It should also be noted that the oxidation step performed by exposing the YH_{2-x} films to air introduces an additional variable, as the relative air composition and, in particular, humidity can influence the oxidation process and, consequently, the film properties. In our experiments, the magnetron sputtering system is located in a clean room environment, which maintains low levels of airborne particles and chemical vapors compared to ambient air. However, the system is not connected to a glove box, and thus, immediately after deposition, the YH_{2-x} films were exposed to the clean room air. While this environment is more controlled than typical laboratory air, we did not actively regulate or monitor the humidity or specific gas composition during oxidation. Therefore, we recognize that variations in air humidity and composition could introduce additional sample-to-sample variability in the oxidation process and, by extension, in the final film properties.

3.1. Structural and photochromic behavior from XRD analysis

Hydrogen content in the film that can be controlled by sputtering parameters such as H_2/Ar gas flow ratio, chamber pressure, substrate temperature, and oxidation atmosphere can strongly influence the XRD pattern. Additionally, film texture and crystallite size can be inferred from peak broadening and intensity ratios. These structural features are critical for understanding the precursor phase before oxidation and its influence on the formation and photochromic performance of YHO.

Broadening and reduced intensity in Fig. 1 suggest the formation of a more disordered and nanocrystalline structure. The degree of oxidation and resulting phase composition can vary depending on environmental conditions and film thickness, with fully oxidized YHO exhibiting distinct diffraction features compared to partially oxidized intermediates. These structural changes are closely linked to the material's photochromic properties, making XRD a vital tool for monitoring phase evolution and optimizing functional performance.

Figure 1 presents X-ray diffraction patterns of the YHO thin films (S3-S8), analyzed alongside reference patterns for metallic yttrium (Y) with a hexagonal close-packed (hcp) lattice and yttrium dihydride (YH_2), obtained from standard PDF cards 00-033-1458 and 04-002-6938, respectively, and previously published works [10, 11]. The YHO reference pattern is based on our earlier Rietveld refinement of the cubic $Fm\bar{3}m$ YHO [25]. This comparative approach enables more precise identification of phase composition and structural variations among the samples.

Our analysis demonstrates that the deposition conditions play a critical role in photochromic performance [13-15] and structural properties of YHO. For example, the XRD patterns show critical insights into the crystallographic texture and its correlation with photochromic activity. The similarity in diffraction patterns among films S3, S4, S6-S8 suggests that these films share a common crystalline phase. More specifically, they are crystallized in the cubic YHO structural arrangement with the space group $Fm\bar{3}m$ (Fig. 1) as reported previously in [25]. Analysis of XRD patterns of the samples (S3, S4, S6-S8) shows that the ratio of intensities between (111) and (200) peaks changes. The variations in intensity ratios between the (111) and (200) reflections indicate differences in preferred orientation or texture, which are influenced by the hydrogen partial pressure during deposition (Table 1). Importantly, films exhibiting a dominant (111) orientation, such as S3 and S6-S8, consistently demonstrate enhanced photochromic behavior. This observation is supported by our experimental results and agrees with literature reports [1, 7], which suggest that the (111) texture may facilitate more efficient hydrogen diffusion and electronic transitions responsible for reversible photodarkening and bleaching. In contrast, films with a pronounced (200) orientation, such as S4, show a diminished photochromic response. Overall, these findings underscore the sensitivity of YHO thin films to deposition parameters, particularly hydrogen pressure, which governs not only phase formation and texture but also key functional properties such as photochromism.

The black-colored film S5 does not exhibit photochromic properties (see inset in Fig. 1). The XRD pattern of S5 closely resembles that of YH_2 [19, 29], which typically crystallizes in a face-centered cubic (fcc) CaF_2-type structure, with yttrium atoms occupying the fcc lattice sites and hydrogen atoms located in the tetrahedral interstitial positions [29]. However, in comparison with the YHO films (S3, S4, S6-S8), the diffraction peaks of S5 are shifted to higher angles. This shift indicates that, while S5 retains the overall fcc structural motif characteristic of YH_2, its lattice parameter is contracted relative to both stoichiometric YH_2 and the YHO films. Such contraction likely arises from partial oxidation and/or reduced hydrogen content in S5, resulting in a denser lattice. Thus, S5 is structurally similar to YH_2 but exhibits a contracted lattice due to its distinct composition.

Analysis of the XRD patterns of YHO thin films (samples S3-S8) reveals that the hydrogen partial pressure during deposition strongly affects the crystallite size D and structural order. Films deposited at intermediate Ar/H_2 ratios as S3 and S6-S8, tend to show broader and less intense diffraction peaks, which are indicative of smaller crystallite sizes (D = 5-6.5 nm) and increased structural disorder. Also, the ratio of intensities between the (111) and (200) reflections changes with hydrogen pressure. Films with a (111) preferential orientation (typically at intermediate Ar/H_2 ratios, e.g., S3 and S6-S8) exhibit enhanced photochromic behavior and are associated with less favorable crystallite growth. In contrast, a shift toward (200) texture (higher Ar/H_2 ratio, e.g., S4) suppresses photochromic activity and may be linked to larger (D = 9.4 nm) crystallites.

Broadening and reduced intensity of XRD peaks suggest a decrease of crystallinity. This is corroborated by EXAFS analysis, which shows that the local atomic environment around yttrium is distorted, with a clear splitting of the second Y-Y coordination shell (double peak at 3.5-4.5 Å). The presence of anion vacancies and compositional deviations from stoichiometry (as seen in S3 and S6-S8) contributes to significant long-range disorder. These defects disrupt the ideal cubic symmetry observed by XRD and are most pronounced in films far from stoichiometry.

To conclude, films with smaller crystallites (preferential (111) orientation) show better photochromic performance. Larger crystallite size and preferential (200) orientation are associated with reduced or absent photochromic activity, as seen in the S4 film.

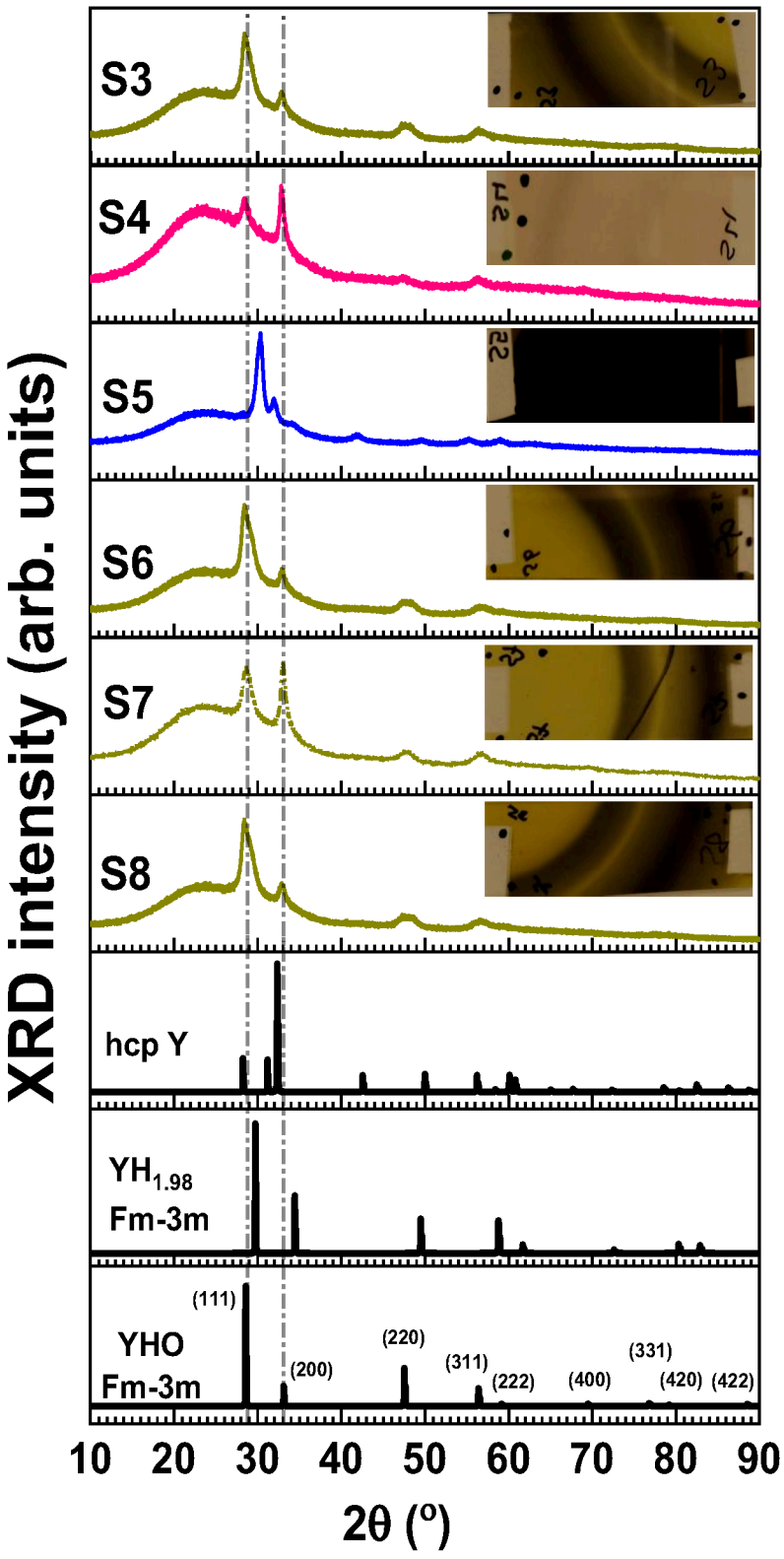

Fig. 1. *X-ray diffraction patterns of the YHO thin films (S3-S8), produced with varying hydrogen content. The XRD patterns of the YHO thin films were acquired from their transparent parts. The XRD pattern of hcp Y (PDF Card - 00-033-1458) and cubic* $Fm\bar{3}m$ *$YH_{1.98}$ (PDF Card - 04-002-6938) and YHO phases are shown for comparison. Photographs of samples after coloration in certain places are shown as insets.*

3.2. Electronic structure insights from XANES Spectroscopy

The Y K-edge XANES spectra provide information about the local electronic structure of yttrium in the thin films, and the absorption edge positions serve as proxies for the oxidation state of yttrium (Fig. 2). The XANES spectra are dominated by the 1*s*(Y)→*np*(Y) dipole-allowed transitions. The energy positions of the absorption edges, evaluated from the first derivative maximum, for the thin films S3, S4, S6-S8 are similar, being close but not equal to that of Y_2O_3. Previously, we found [19] that such a position of the absorption edge corresponds to an effective oxidation state of yttrium ions of about +2.5. This is consistent with the presence of the YHO phase, where yttrium is oxidized due to its bonding with both oxygen and hydrogen. It is noticeable that upon photodarkening, the edge position does not change in all samples, which indicates that the oxidation state of Y cations in the samples S3, S4, S6-S8 does not change. This result is consistent with XANES and EXAFS analyses [9, 10], suggesting that photochromism in YHO is not associated with a change in the average oxidation state of yttrium cations. Consequently, the reduction of Y^{3+} to Y^{2+} [12] observed by nuclear magnetic resonance (NMR) spectroscopy might be related to light-induced anion vacancy formation and defect diffusion.

In contrast, sample S5 exhibits a significantly lower edge energy position, evaluated from the first derivative maximum, corresponding to an effective oxidation state of yttrium ions of about +0.9 as compared to +2.5 characteristic of the samples S3, S4, S6-S8 [19]. This suggests a mixture of the black color metallic yttrium hydride and metallic yttrium phases in S5, which lacks the oxidized character necessary for photochromic functionality. The absence of the edge shift upon illumination further confirms that the electronic structure of the sample S5 remains unaltered, reinforcing the conclusion that the oxidation state of Y cations is not modified by illumination.

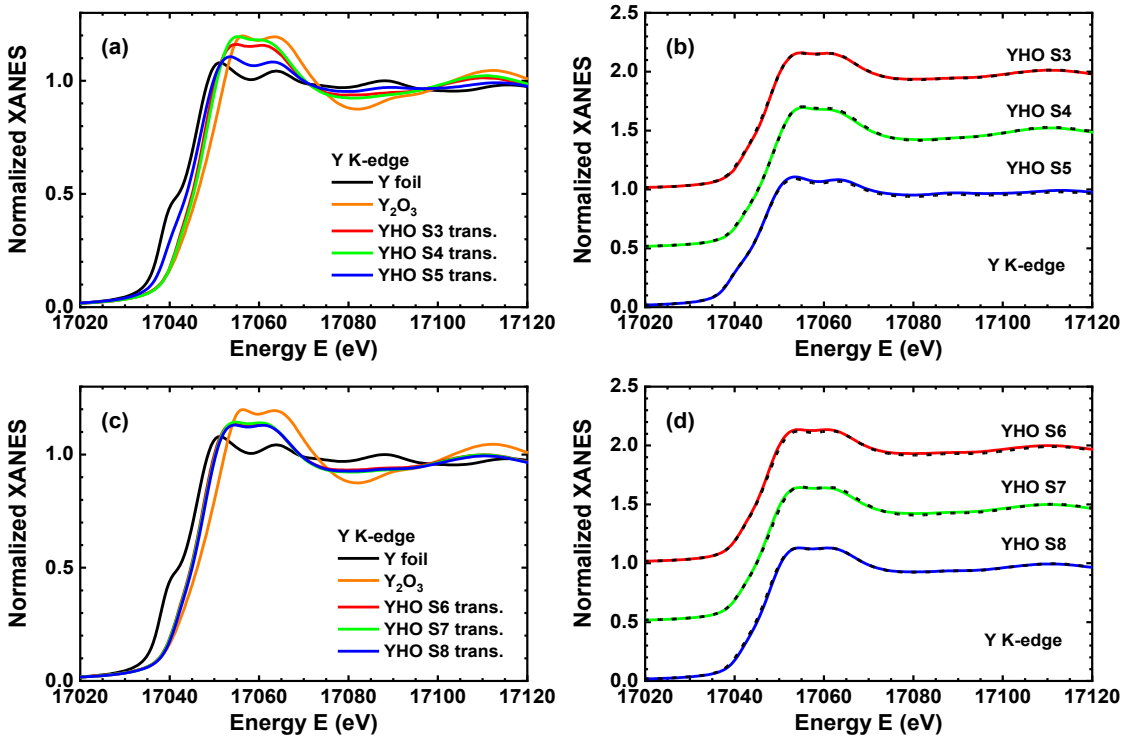

Fig. 2. *Experimental Y K-edge XANES spectra of the YHO thin films (S3-S8): (a, c) comparison with two reference compounds Y_2O_3 and Y foil, (b, d) comparison between spectra for transparent (solid curves) and photodarkened (dashed curves) states.*

3.3. Structural insights from EXAFS spectroscopy

EXAFS spectroscopy at the Y K-edge provides valuable information about the local atomic environment surrounding yttrium atoms in the YHO thin films. Figure 3 displays the experimental Y K-edge EXAFS spectra $\chi(k)k^2$ for transparent YHO thin films (S3-S8) as compared to the reference compounds Y_2O_3 and Y foil. The similarity between the EXAFS spectra of samples S3 and S4 and those of samples S6, S7, and S8 suggests a similar local coordination environment around yttrium in these films. At low wavenumber values ($k < 4$ Å^{-1}), their EXAFS spectra resemble the spectrum of cubic Y_2O_3 powder. However, the EXAFS spectrum of yttria has a stronger amplitude at large k-values, indicating lower structural disorder. The EXAFS spectrum of sample S5 deviates significantly from those of the other films (Fig. 3(a)). Its oscillation pattern changes in the direction of that of metallic yttrium foil, indicating a metallic-like environment with reduced oxygen coordination, which correlates with its phase composition determined by XRD.

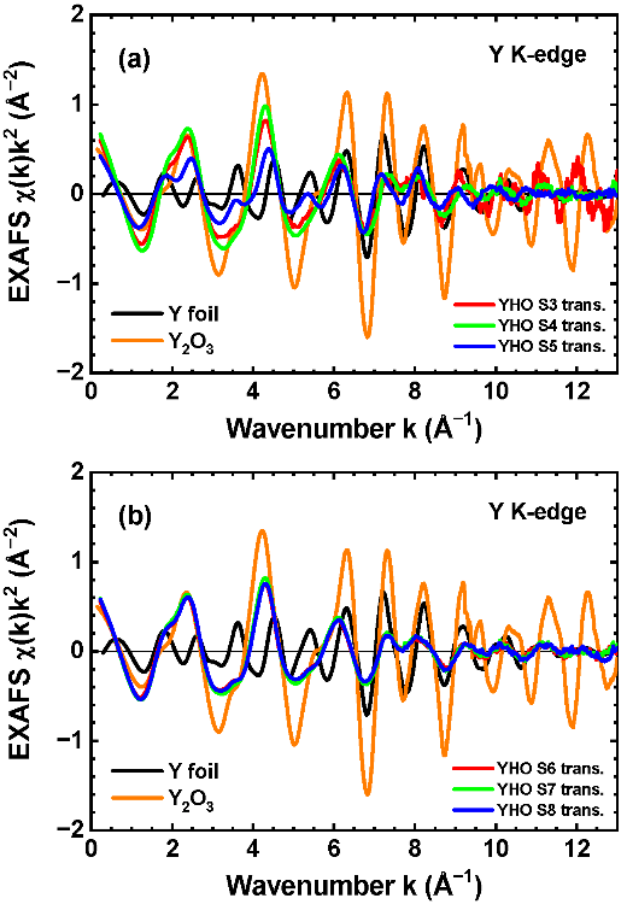

Fig. 3. *Experimental Y K-edge EXAFS spectra $\chi(k)k^2$ of the (a) S3-S5 and (b) S6-S8 YHO films in transparent state as compared to two reference compounds Y_2O_3 and Y foil.*

The Y K-edge EXAFS spectra $\chi(k)k^2$ and their Fourier Transforms (FTs) for all films in the transparent and dark states are shown in Fig. 4. The color change is accompanied by similar, albeit small, changes in the local environment, as evidenced by variations in the first and second peaks of the FTs. This effect is most pronounced in samples S6–S8, smaller in S3 and S4, and absent in S5. Similar behavior was previously observed by us in selected photochromic YHO powders and films [9, 19, 25].

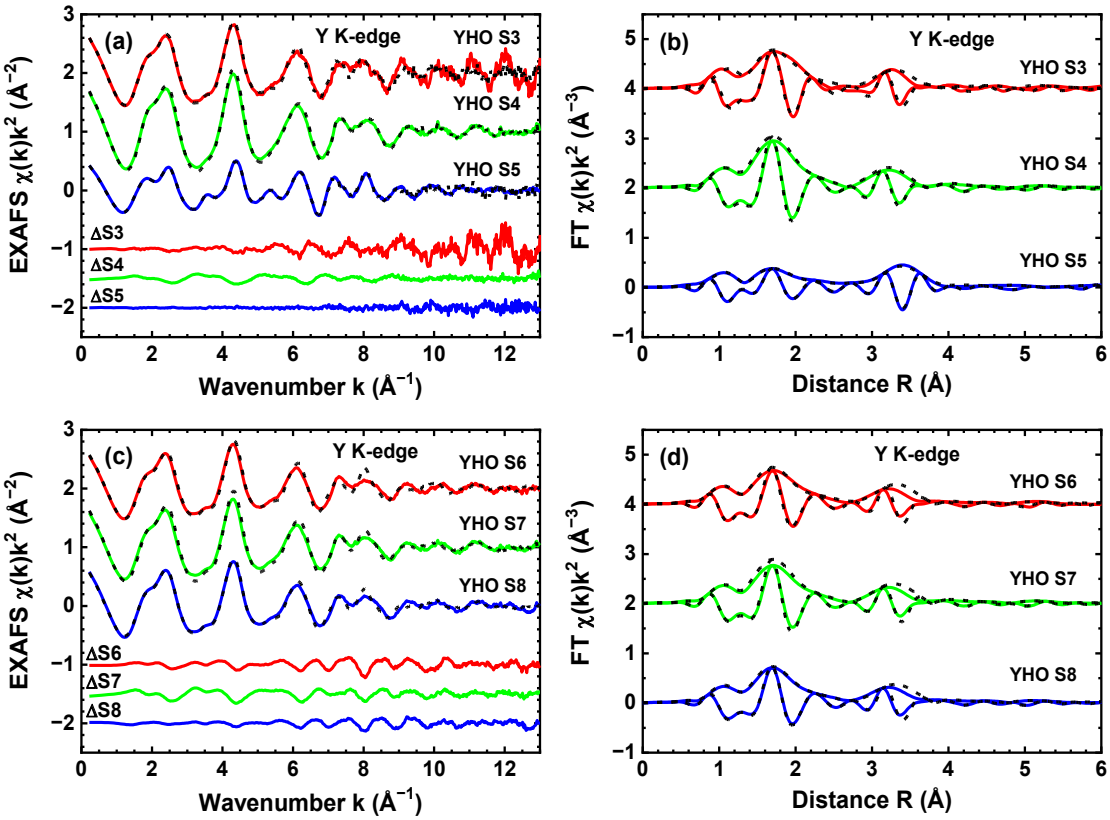

Fig. 4. *Experimental (a), (c) Y K-edge EXAFS spectra $\chi(k)k^2$ and (b), (d) their Fourier transforms (FTs) of the (a), (b) S3-S5 and (c), (d) S6-S8 YHO thin films in transparent (solid curves) and photodarkened (dashed curves) states. The differences between the EXAFS spectra in transparent and photodarkened states are shown in (a) and (c) as ΔS3-ΔS8. Both the moduli and imaginary parts of the FTs are shown.*

To elucidate the structural origin of the observed changes, the EXAFS spectra of all films were analyzed using the RMC method [23, 24]. An example of the RMC simulation for sample S6 is shown in Fig. 5, with comparable fit quality obtained for samples S3, S4, S7, and S8. Note that the RMC fit was performed in the wavelet space by minimizing the difference between the wavelets of the experimental and RMC-calculated Y K-edge EXAFS spectra. Good agreement between the experimental and calculated EXAFS spectra is observed in both *k*- and *R*-spaces as well as in the wavelet space, suggesting that the RMC model effectively captures the local structure around yttrium atoms. Note that the obtained structural model is able to reproduce well the contributions from distant coordination shells up to about 6 Å (Fig. 5(b)).

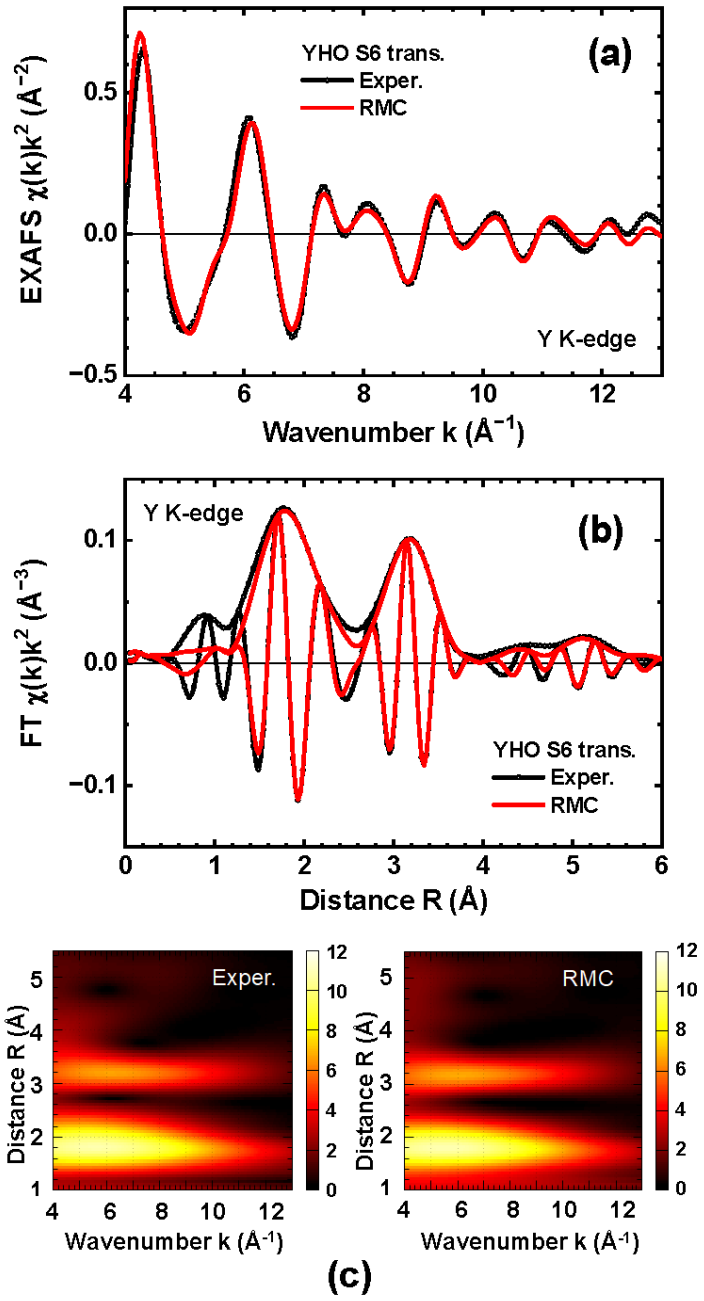

Fig. 5. *Comparison of the experimental and RMC-calculated Y K-edge EXAFS spectra $\chi(k)k^2$ (a) and their Fourier (b) and Morlet wavelet (c) transforms for the YHO S6 thin film in the transparent state. Both the moduli and imaginary parts of the FTs are shown.*

The coordinates of atoms in the RMC simulation box were used to calculate the partial radial distribution functions (RDFs) g(*r*) Y-O and Y-Y for YHO films in the transparent and dark states. They are presented for selected YHO thin films S4 (Fig. 6(a)), S6 (Fig. 6(b)), S7 (Fig. 6(c)), and S8 (Fig. 6(d)). A splitting of the second shell (double peak at 3.5-4.5 Å) is clearly observed in all cases and is most affected by photocoloration. Specifically, an increase in the peak amplitude at 3.6 Å is observed in all samples, being largest in S6.

A detailed explanation of the second shell splitting was provided by us recently in [9, 25]. It was shown that, despite XRD indicating a cubic $Fm\bar{3}m$ symmetry for the YHO lattice (Fig. 1), the local environment of yttrium ions is distorted due to the presence of anion vacancies [9,

25]. Since the S4, S6, S7, and S8 samples are compositionally different and are far from stoichiometry, a large concentration of defects is expected in the sample.

A detailed comparison of the partial Y-O and Y-Y RDFs (Fig. 6) in the transparent and photodarkened states suggests small changes in peak broadening, at least in the first (peak at 2-3 Å) and second (peak at 3.3-4.4 Å) coordination shells of yttrium. This result correlates with a change in the charge state of anion vacancies [9], which occurs under the photochromic effect and leads to lattice relaxation. In fact, strong lattice relaxation in the presence of anion vacancies was demonstrated in YHO by DFT simulations in [9], which predicted light-induced lattice contraction and expansion.

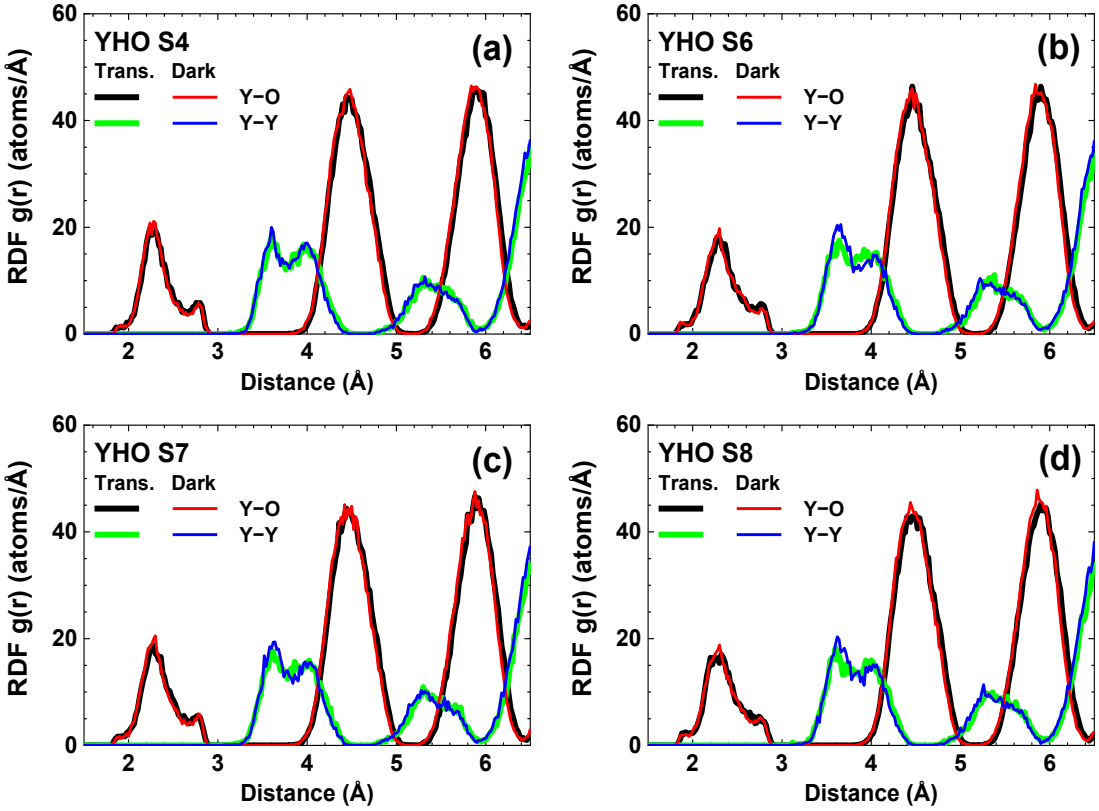

Fig. 6. *Partial radial distribution functions (RDFs) g(r) for Y–O and Y–Y for selected YHO thin films (a) S4, (b) S6, (c) S7, amd (d) (S8) in transparent (thick solid curves) and dark (thin solid curves) states, obtained using the RMC method from the Y K-edge EXAFS spectra. The splitting of the second yttrium shell into two groups of yttrium atoms (peaks at about 3.6 Å and 4.0 Å) is visible.*

4. Conclusions

A systematic structural study of the impact of hydrogen concentration on the local structural arrangement and oxidation state of yttrium cations was performed for the transparent and photodarkened states of photochromic YHO thin films deposited by DC magnetron sputtering. Analysis of the X-ray diffraction patterns suggests that an increase in the Ar/H_2 ratio strongly influences the texture and phase composition of the films. Good photochromic activity is observed in YHO films with a preferential (111) orientation, whereas the photochromic activity is reduced when the film texture shifts toward a preferential (200) orientation.

The Y K-edge X-ray absorption spectroscopy studies indicate that the effective yttrium oxidation state of about +2.5 remains unchanged in both transparent and photocolored YHO films and is not affected by reasonable tuning of the chamber pressure and Ar/H_2 ratio, nor by

UV illumination. However, at sufficiently high Ar/H_2 ratios, the films lose their photochromic properties due to the appearance of yttrium hydride and metallic phases. Note that all thin films with photochromic response have also slightly different Y K-edge EXAFS spectra in the transparent and dark states. Their detailed analysis using the RMC method indicates that the local atomic structure around yttrium is distorted, with a clearly observed splitting of the second Y-Y coordination shell. Moreover, we found that the changes in the Y K-edge EXAFS spectra upon photocoloration affect, at least, the first and second coordination shells of yttrium. These findings reinforce the critical role of local atomic structure in governing the photochromic properties of YHO thin films.

Acknowledgements

The work by HA and SAK was funded by Latvian Council of Science Project No. lzp-2024/1-0632. Also, funding was provided by SWEB project 101087367 funded by the HORIZON-WIDERA-2022-TALENTS-01-01. We acknowledge DESY (Hamburg, Germany), a member of the Helmholtz Association HGF, for the provision of experimental facilities. Parts of this research were carried out at the DESY PETRA III synchrotron, and we would like to thank Dr. Edmund Welter for assistance in using the P65 beamline. Beamtime was allocated for proposal I-20230822 EC.

References

[1] T. Mongstad, C. Platzer-Björkman, J. P. Maehlen, L. P. A. Mooij, Y. Pivak, B. Dam, E. S. Marstein, B. Hauback, S. Z. Karazhanov, A new thin film photochromic material: Oxygen-containing yttrium hydride, Solar Energy Mater. Solar Cells. **95**, 3596–3599 (2011).

[2] J. Montero, F. A. Martinsen, M. García-Tecedor, S. Z. Karazhanov, D. Maestre, B. Hauback, E. S. Marstein, Photochromic mechanism in oxygen-containing yttrium hydride thin films: An optical perspective, Phys. Rev. B **95**(20), 201301 (2017).

[3] S. K. Deb, Optical and photoelectric properties and colour centres in thin films of tungsten oxide, Phil. Mag. **27**(4), 801–822 (1973).

[4] S. K. Deb, J. A. Chopoorian, Optical properties and color-center formation in thin films of molybdenum trioxide, J. Appl. Phys. **37**(13), 4818–4825 (1966).

[5] S. Deb, L. Forrestal. Photochromism in inorganic systems. In: Photochromism. Techniques of Chemistry, Vol. III. Ed. G.H. Brown, Wiley-Interscience, 1971, pp. 633–665.

[6] J. Montero-Amenedo, Photochromism in rare earth oxyhydrides for large-area transmittance control, Solar Energy Mat. Solar Cells. **272**, 112900 (2024).

[7] C. C. You, T. Mongstad, J. P. Maehlen, S. Karazhanov, Dynamic reactive sputtering of photochromic yttrium hydride thin films, Solar Energy Mater. Solar Cells. **143**, 623–626 (2015).

[8] W. Wang, Y. Cheng, X. Xie, Design and applications of photochromic compounds for quantitative chemical analysis and sensing, Chem. Commun. **61**(46), 8327–8338 (2025).

[9] H. Arslan, A. Kuzmin, K. Vinoth Kumar, I. Aulika, D. Moldarev, D. Primetzhofer, M. Wolff, I. Pudza, Ø. Nordseth, S. Z. Karazhanov, Anion vacancy-induced photochromism and lattice relaxation in yttrium oxyhydride, Commun. Mater. **6**, 154 (2025).

[10] H. Arslan. PhD, *Mechanism of Photochromism in yttrium oxyhydride and growth kinetics of yttrium oxide thin films*. Riga: University of Latvia. (2025).

[11] E. M. Baba, J. Montero, E. Strugovshchikov, E. Ö. Zayim, S. Karazhanov, Light-induced breathing in photochromic yttrium oxyhydrides, Phys. Rev. Mater. **4**(2), 025201 (2020).

[12] B. Dam, F. Nafezarefi, D. Chaykina, G. Colombi, Z. Wu, S. W. H. Eijt, S. Banerjee, G. de Wijs, A. Kentgens, Perspective on the photochromic and photoconductive properties of rare-earth oxyhydride thin films, Solar Energy Mater. Solar Cells. **273**, 112921 (2024).

[13] D. Moldarev, D. Primetzhofer, C. C. You, S. Z. Karazhanov, H. Palonen, J. Montero, F. Martinsen, T. Mongstad, E. S. Marstein, M. Wolff, Composition of photochromic oxygen-containing yttrium hydride films, Solar Energy Mater. Solar Cells. **177**, 66–69 (2018).

[14] C. C. You, D. Moldarev, T. Mongstad, D. Primetzhofer, M. Wolff, E. S. Marstein, S. Z. Karazhanov, Enhanced photochromic response in oxygen-containing yttrium hydride thin films transformed by an oxidation process, Solar Energy Mater. Solar Cells. **166**, 185–189 (2017).

[15] D. Moldarev, M. V. Moro, C. C. You, E. M. Baba, S. Z. Karazhanov, M. Wolff, D. Primetzhofer, Yttrium oxyhydrides for photochromic applications: Correlating composition and optical response, Phys. Rev. Mater. **2**(11), 115203 (2018).

[16] S. Cornelius, G. Colombi, F. Nafezarefi, H. Schreuders, R. Heller, F. Munnik, B. Dam, Oxyhydride nature of rare-earth-based photochromic thin films, J. Phys. Chem. Lett. **10**(6), 1342–1348 (2019).

[17] G. Colombi, T. De Krom, D. Chaykina, S. Cornelius, S. W. H. Eijt, B. Dam, Influence of cation (RE = Sc, Y, Gd) and O/H anion ratio on the photochromic properties of REO_xH_{3-2x} thin films, ACS Photonics **8**(3), 709–715 (2021).

[18] F. A. Martinsen, J. A. Montero, S. Z. Karazhanov, T. T. Mongstad, E. Marstein. WO2017125573A1 Fabrication Method for a Photochromic Device (2017).

[19] H. Arslan, A. Kuzmin, I. Aulika, D. Moldarev, M. Wolff, D. Primetzhofer, I. Pudza, K. Kundzins, A. Sarakovskis, J. Purans, S. Z. Karazhanov, Chemical state and atomic structure in stoichiovariants photochromic oxidized yttrium hydride thin films, Z. fur Phys. Chem. **238**, 2075-2100 (2024).

[20] E. Welter, R. Chernikov, M. Herrmann, R. Nemausat, A beamline for bulk sample x-ray absorption spectroscopy at the high brilliance storage ring PETRA III, AIP Conf. Proc. **2054**(1), 040002 (2019).

[21] A. Kalinko. XAESA v.0.07 2023 [Available from: https://gitlab.desy.de/aleksandr.kalinko/xaesa.

[22] A. Kuzmin, J. Chaboy, EXAFS and XANES analysis of oxides at the nanoscale, IUCrJ **1**(6), 571–589 (2014).

[23] J. Timoshenko, A. Kuzmin, J. Purans, Reverse Monte Carlo modeling of thermal disorder in crystalline materials from EXAFS spectra, Comp. Phys. Commun. **183**(6), 1237–1245 (2012).

[24] J. Timoshenko, A. Kuzmin, J. Purans, EXAFS study of hydrogen intercalation into ReO_3 using the evolutionary algorithm, J. Phys.: Condens. Matter **26**(5), 055401 (2014).

[25] H. Arslan, I. Pudza, A. Kuzmin, S. Karazhanov, Evidence of local structural distortions and subtle thermal disorder in transparent photochromic yttrium oxyhydride, Appl. Phys. Lett. **124**(15), 151901 (2024).

[26] I. Jonane, K. Lazdins, J. Timoshenko, A. Kuzmin, J. Purans, P. Vladimirov, T. Gräning, J. Hoffmann, Temperature-dependent EXAFS study of the local structure and lattice dynamics in cubic Y_2O_3, J. Synchrotron Radiat. **23**(2), 510–518 (2016).

[27] J. Timoshenko, A. Kuzmin, Wavelet data analysis of EXAFS spectra, Comp. Phys. Commun. **180**(6), 920–925 (2009).

[28] A. L. Ankudinov, B. Ravel, J. J. Rehr, S. D. Conradson, Real-space multiple-scattering calculation and interpretation of x-ray-absorption near-edge structure, Phys. Rev. B **58**(12), 7565-7576 (1998).

[30] D. L. Uhrich, Measurement of the lattice constant in the dihydrides of gadolinium-yttrium alloys, J. Chem. Phys. **44**(5), 2202–2203 (1966).